ARTICLES
PUBLISHED ONLINE: 2 FEBRUARY 2014 | DOI: 10.1038/NCHEM.1861
nature chemistry

Dye-sensitized solar cells with 13% efficiency achieved through the molecular engineering of porphyrin sensitizers

Simon Mathew[1†], Aswani Yella[1†], Peng Gao[1], Robin Humphry-Baker[1], Basile F. E. Curchod[2], Negar Ashari-Astani[2], Ivano Tavernelli[2], Ursula Rothlisberger[2], Md. Khaja Nazeeruddin[1] and Michael Grätzel[1]*

Dye-sensitized solar cells have gained widespread attention in recent years because of their low production costs, ease of fabrication and tunable optical properties, such as colour and transparency. Here, we report a molecularly engineered porphyrin dye, coded SM315, which features the prototypical structure of a donor–π-bridge–acceptor and both maximizes electrolyte compatibility and improves light-harvesting properties. Linear-response, time-dependent density functional theory was used to investigate the perturbations in the electronic structure that lead to improved light harvesting. Using SM315 with the cobalt(II/III) redox shuttle resulted in dye-sensitized solar cells that exhibit a high open-circuit voltage V_{OC} of 0.91 V, short-circuit current density J_{SC} of 18.1 mA cm^{-2}, fill factor of 0.78 and a power conversion efficiency of 13%.

Dye-sensitized solar cells (DSCs) are an attractive solar energy conversion technology and their advantages include their low cost of manufacture, ease of fabrication and modifiable aesthetic features, such as colour and transparency[1–4]. Initial forms of this technology employed ruthenium(II)-based dyes in conjunction with iodide-based electrolytes to achieve a certified solar-to-electric power conversion efficiency (PCE) of 11.9% under full sun illumination (AM 1.5G, 1,000 W m^{-2})[5]. Surpassing the 12% PCE threshold required a paradigm shift in the chemical components utilized within this photo-electrochemical device[6].

A new generation of DSCs is based on a combination of light-harvesting donor–π–acceptor (D–π–A) dyes in conjunction with cobalt-based redox mediators[6–9]. The strong molar absorptivity of D–π–A dyes enables the use of thin TiO_2 films, potentially reducing fabrication costs relative to ruthenium(II) sensitizers, with concomitant improvements in the open-circuit voltage V_{OC} when used with cobalt-based redox mediators. The synthetic flexibility of D–π–A dyes has enabled the engineering of enhanced compatibility toward these alternative redox couples by introducing steric bulk into the donor component and π-system, minimizing the unfavourable recombination between the electrolyte and the TiO_2 surface[6–9]. By using these new light harvesters, DSCs have achieved a maximum PCE of 12.3% under full sun illumination, utilizing the tris(2,2′-bipyridyl)cobalt(II/III) ($[Co(bpy)_3]^{2+/3+}$) redox shuttle. However, to achieve this PCE, the light harvesting of the porphyrin dye YD2-o-C8 was supplemented by the organic co-sensitizer Y123 (ref. 6). This landmark result began a renaissance for the DSC, validating the combination of D–π–A dyes and cobalt redox mediators as an effective strategy in developing high-efficiency DSCs[10].

The development of single-molecule panchromatic D–π–A sensitizers remains a molecular engineering challenge in efforts to improve the overall PCE of DSC devices. Until now, achieving a panchromatic light-harvesting response in DSCs has relied on co-sensitization, energy-relay strategies or tandem device configurations[6,11–21]. Although gains in PCE are often realized through improved light harvesting utilizing these strategies, the fabrication and optimization of these devices can be laborious and technically challenging. The development of a single D–π–A sensitizer with a panchromatic light response in a DSC remains a main objective in the realization of maximum PCEs with standard device fabrication protocols[6,22].

Porphyrin-based D–π–A dyes provide a highly flexible platform for the development of panchromatic sensitizers[6,23,24]. The porphyrin chromophore has intrinsically strong light absorption in the Soret and Q-bands, but there is a lack of significant absorption in the spectral region between these two features. Typical porphyrin D–π–A sensitizers comprising dialkylamine or diarylamine donors, in conjunction with an ethynylbenzoic acid acceptor, yield dyes with a vivid green colour, bereft of absorption between 500–600 nm (refs 6,24–29). Despite the high efficiency of these dyes in DSCs, further improvements to light harvesting through the use of stronger acceptors remains relatively unexplored[30,31]. Studies unrelated to the DSC have demonstrated that integration of proquinoidal units into the porphyrin structure causes strong perturbations to the electronic structure of the macrocycle[32–35]. These perturbations in benzothiadiazole–porphyrin analogues result in improved light harvesting by broadening and redshifting absorbance of the Soret and Q-bands.

In this work, we reengineered the prototypical structure of D–π–A porphyrins to simultaneously maximize cobalt–electrolyte compatibility and improve the light-harvesting properties. Functionalization of the porphyrin core with the bulky bis(2′,4′-bis(hexyloxy)-[1,1′-biphenyl]-4-yl)amine[36] donor and a 4-ethynylbenzoic acid yielded the green dye SM371, which exhibited a slightly improved PCE of 12% compared to the previously reported YD2-o-C8 (11.9%)[6]. Incorporation of the proquinoidal benzothiadiazole (BTD) unit into this structure afforded the dye SM315, a panchromatic porphyrin sensitizer (Fig. 1). SM315 exhibited

[1]Laboratory of Photonics and Interfaces (LPI), École Polytechnique Fédérale de Lausanne (EPFL), CH-1015, Lausanne, Switzerland, [2]Laboratory of Computational Chemistry and Biochemistry (LCBC), École Polytechnique Fédérale de Lausanne (EPFL), CH-1015 Lausanne, Switzerland; †These authors contributed equally to this work. *e-mail: michael.graetzel@epfl.ch

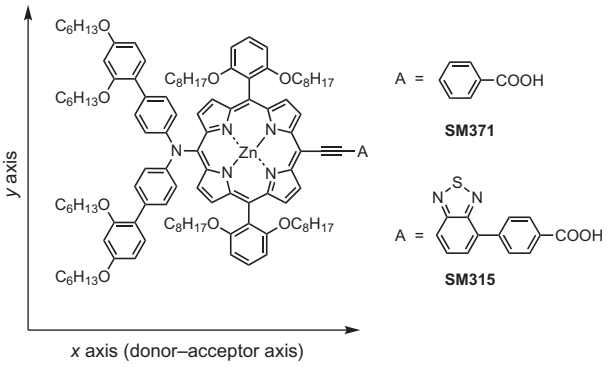

Figure 1 | Structures of the two dyes used in the study. The structures are coded **SM371** and **SM315**. They both feature a porphyrin core and a bulky bis(2′,4′-bis(hexyloxy)-[1,1′-biphenyl]-4-yl)amine donor. Their acceptor groups differs, with **SM315** featuring a benzothiadiazole group.

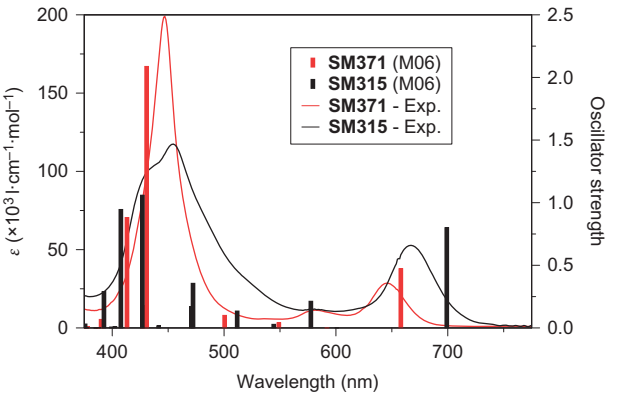

Figure 2 | Absorption spectra of the dyes studied. The experimental spectra (in THF) are shown as continuous lines and the theoretical electronic transitions are shown as bars for both **SM371** (red) and **SM315** (black). Theoretical data were computed using LR-TDDFT/M06/IEF-PCM(THF).

significant broadening of Soret and Q-band absorbance features compared to **SM371**, yielding improved light harvesting in both the green (500–600 nm) and red (up to 800 nm) region of the spectrum. **SM315** demonstrated an enhancement in green light absorption, resulting in an improved J_{SC} (18.1 versus 15.9 mA cm^{-2} for **SM315** and **SM371**, respectively) when utilized in the DSC. Ultimately, the panchromatic sensitizer **SM315** achieved a record 13.0% PCE at full sun illumination without the requirement of a co-sensitizer.

Results and discussion

Opto-electronic properties of the porphyrin sensitizers. The syntheses of the dyes **SM371** and **SM315** are provided in the Supplementary Information. The donor group bis(2′,4′-bis(hexyloxy)-[1,1′-biphenyl]-4-yl)amine was specifically used in the two dyes as it has demonstrated compatibility with cobalt-based electrolytes and yields high open-rcircuit photovoltages[7–9,36]. Table 1 summarizes the UV–vis, fluorescence and cyclic voltammetry data for **SM371** and **SM315**.

Figure 2 shows the solution (THF) absorption spectra of the **SM371** and **SM315** sensitizers. **SM371** features an absorption spectrum typical of porphyrins functionalized with a diarylamine donor and ethynylbenzoic acid acceptor, with maxima from the Soret band (B-band) at 447 nm and from the Q-bands at 580 nm and 646 nm. The introduction of the BTD acceptor unit had a significant impact on the absorption spectrum of **SM315**, most evident by the splitting of the Soret band, resulting in a shoulder at 440 nm on the maximum at 454 nm. Furthermore, the absorption of **SM315** between the Soret and Q-bands (450–550 nm) displayed significant enhancement compared to **SM371**, leading to the panchromatic character of the BTD-functionalized dye. The Q-band at 581 nm remained relatively constant compared to that of **SM371**, but the lowest-energy Q-band absorption of **SM315** was significantly redshifted to 668 nm. Both the spectral splitting and the redshifting of absorbance maxima for **SM315** are consistent with previously reported porphyrin–BTD ensembles[32,37].

Table 1 | Optical and electrochemical data for SM371 and SM315.

Dye	λ_{abs} (nm)/ε (10^3 M^{-1}cm^{-1})	λ_{em} (nm)*	$E_{0\text{-}0}$ (eV)†	E_{ox1} (V)	E_{red1} (V)
SM371	447/199, 580/12, 646/29	674	1.88	0.89	−1.21
SM315	440/105, 454/117, 581/12, 668/53	732	1.79	0.88	−0.99

*Emission maxima obtained in THF by excitation at 440 nm.
†Zero–zero excitation energy, determined by the intersection of normalized absorbance and emission spectra.

The splitting of the Soret band in **SM315** can be rationalized using point-dipole exciton coupling theory[37]. The Soret band (B-band) is a composition of two perpendicularly polarized transitions within the molecule, denoted B_x and B_y, where the x-axis has the greatest degree of conjugation (that is, the donor–acceptor axis, Fig. 1)[38,39]. In a symmetrical zinc tetraphenylporphyrin the B_x and B_y transitions are degenerate. Functionalization of the porphyrin with donor and acceptor moieties to afford **SM371** increased the conjugation and charge transfer (CT) character along the donor–acceptor axis (that is, x-axis) of the dye, causing the Soret absorption originating from the B_x transition to be redshifted with increased molar absorptivity. Overall, the Soret band in **SM371** appears both broad and redshifted, as the B_x and B_y transitions are no longer degenerate. The presence of the BTD-functionalized acceptor in **SM315** further increased the electronic asymmetry and CT character of the dye, causing a redshifted B_x transition, which resulted in the Soret band appearing as two distinguishable maxima in the absorbance spectrum. Furthermore, the presence of the BTD acceptor increased the x-axis polarizability of **SM315**, indicative of increased oscillator strength for the B_x transition, rationalizing the differences in molar absorptivity between the two Soret maxima.

Another noticeable difference in the spectra of the two dyes is the redshift and increase in molar absorptivity of the lowest-energy Q-band for **SM315**. For both dyes, the absorbance originating from the Q_y transition remains relatively unperturbed, appearing at 580 nm and 581 nm in **SM315** and **SM371**, respectively. The increased conjugation along the x-axis of **SM315** strongly shifted absorbance from the Q_x transition to produce a maximum at 668 nm. The significant increase in molar absorption coefficient is consistent with the increased oscillator strength of the Q_x transition from enhanced x-axis polarizability within the **SM315** upon introduction of the BTD unit.

Comparison of the frontier Kohn–Sham (KS) orbitals between the two compounds highlighted the effect of the BTD acceptor on the electronic structure of **SM315** (Fig. 3). The KS highest occupied molecular orbital (HOMO) of both dyes was predominantly localized on the donor and was not affected by the choice of acceptor. The location of the KS lowest unoccupied molecular orbital (LUMO) in **SM315** demonstrated a significant shift towards the BTD component of the acceptor. Hence, the electronic transition in **SM315** with a dominant HOMO → LUMO contribution was expected to exhibit an enhanced CT character compared to **SM371**.

The calculated absorption spectra for **SM371** and **SM315** (Fig. 2) were obtained by using linear-response time-dependent density functional theory (LR-TDDFT) and the M06 functional[40]. An integral equation formalism of the polarizable continuum model (IEF-PCM) with a relative permittivity of 7.43 was used to simulate the solvent (THF) used for the experimental absorption data (see Supplementary Information for full computational details and a discussion of the protocol used). The LR-TDDFT/M06/IEF-PCM(THF) methodology predicted a strong alteration of the Soret band for **SM315**, with two distinct transitions appearing at 408 nm and 427 nm (3.04 and 2.90 eV, respectively), with similar oscillator strengths, consistent with the splitting observed experimentally, which contributes to the panchromatic character of the dye. Analysis of the transition density difference plots (Supplementary Fig. 2) for the two Soret transitions of **SM315** revealed that the lower-energy Soret absorption exhibited a significant contribution from the BTD acceptor (that is, greater polarizability along the donor–acceptor axis due to an enhanced CT character), consistent with the rationalization provided from point-dipole exciton coupling theory (*vide supra*). In contrast, the LR-TDDFT/M06/IEF-PCM(THF) absorption spectra of **SM371** indicated that the Soret band is dominated by a strong transition at 431 nm and a weaker second transition computed at 413 nm, reproducing the trends in Soret band splitting observed experimentally between the two dyes.

The calculated absorption of **SM315** presented a vertical transition with moderate oscillator strength (0.213) at 578 nm (2.15 eV), with significant donor-to-acceptor character (HOMO-1 → LUMO, 83%). This small absorption, in line with the experimental observation, also contributes to the enhanced panchromatic light-harvesting ability of **SM315**, together with a series of absorption lines between 601 nm and 430 nm. The calculated absorption spectra afforded a first vertical excitation at 658 nm (1.88 eV) and 699 nm (1.77 eV) for **SM371** and **SM315**, respectively, consistent with the experimental values of 646 nm (1.92 eV) and 668 nm (1.86 eV) for the lowest-energy Q-bands. For both dyes, this first electronic transition is characterized by a dominant HOMO → LUMO contribution of comparable magnitude, 91% for **SM371** and 88% for **SM315**, confirming the CT character of both dyes (further supported by transition density plots; Supplementary Figs 1,2). The presence of the BTD moiety in **SM315** results in an extended delocalization of the LUMO onto this acceptor site, enhancing the CT character of this band, together with a shift towards lower energy and higher oscillator strength. The second transition is computed at a similar energy for both dyes, 600 nm (**SM315**) and 592 nm (**SM371**), and displays in both cases small oscillator strength and a similar character (Supplementary Figs 1 and 2).

Characterization of the surface-mounted dyes was achieved by adsorbing the sensitizer onto a 1-μm-thick TiO_2 substrate following acquisition of a Fourier transform infrared (FTIR) spectrum (Supplementary Fig. 3). On adsorption to TiO_2, the FTIR spectra revealed the disappearance of the carbonyl stretch, ν(C=O), at 1,690 cm^{-1} from the neat dye, with a concomitant increase in the intensity of the band at 1,380 cm^{-1}, which originates from the symmetric carboxylate band, $\nu(COO^{-}_{sym})$. This change is characteristic of bidentate binding by both oxygen atoms of the carboxylate functional group to the titania of the substrate, consistent with previous reports[41–43].

UV–vis characterization of the surface-mounted dyes was achieved by adsorbing the sensitizer onto a 1-μm-thick TiO_2 substrate (data presented in the Supplementary Information; Supplementary Fig. 4). Both dyes experienced a slight blueshift on adsorption to the titania, which was attributed to the decrease in dipole following loss of the carbonyl moiety of the anchoring group, consistent with observations from FTIR analysis of the substrate. The degrees of blueshift for absorptions derived from the B_y and Q_y transitions were less than for those derived from the B_x and Q_x transitions, consistent with the rationale provided by point-dipole exciton coupling theory (*vide supra*). Measurement of the light-harvesting efficiency (LHE) of **SM371** and **SM315** on transparent TiO_2 films (3.5 μm) is provided in the Supplementary Information (Supplementary Fig. 5). The LHEs for **SM371** and **SM315** exhibited maxima that correlated with those observed in the experimental absorption spectrum. Measurement of LHE revealed that **SM315** has a near-quantitative LHE throughout the

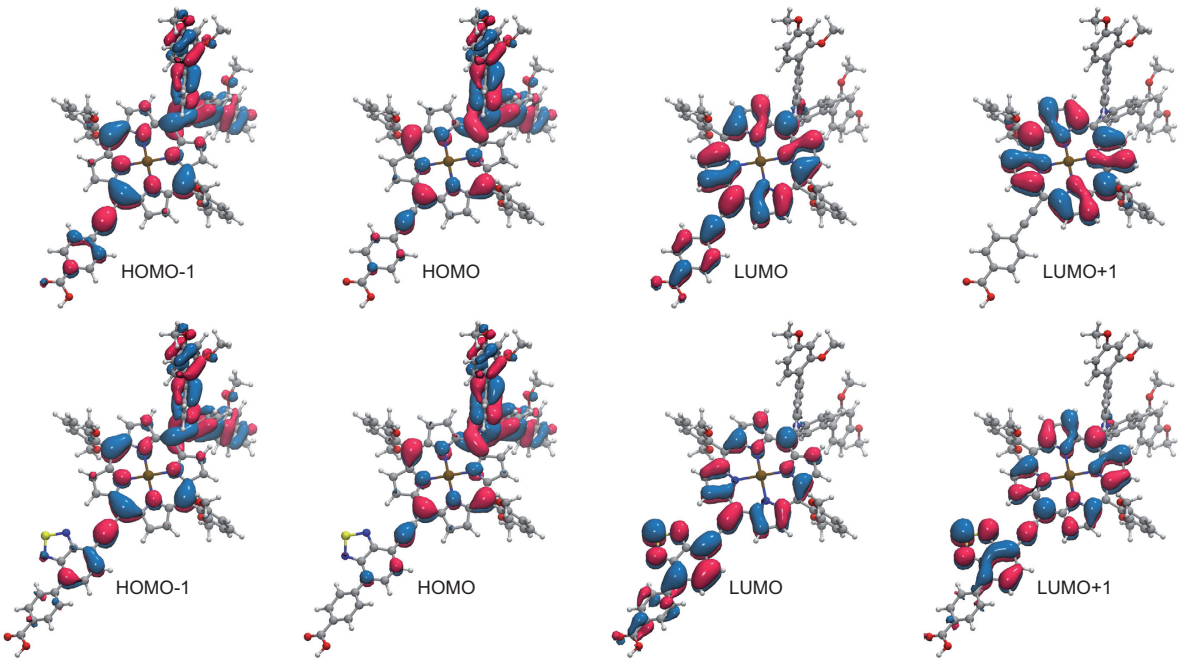

Figure 3 | Contour plots of selected KS orbitals for the dyes studied. The orbitals were calculated for geometry-optimized **SM371** (top) and **SM315** (bottom), using DFT/M06/IEF-PCM(THF). (Isovalue set to 0.02 a.u.).

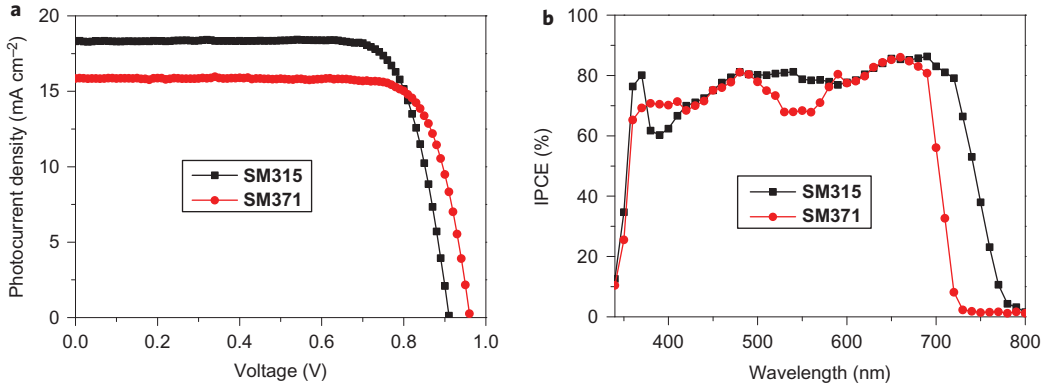

Figure 4 | Photovoltaic performance of devices made with SM371 and SM315. a, *J–V* curve under AM 1.5G illumination (1,000 W m^{-2}) and **b**, photocurrent action spectrum for **SM371** (red) and **SM315** (black).

visible region, which is a dramatic improvement over **SM371**. The splitting and redshifting of Soret and Q-band absorptions upon introduction of the BTD unit into the dye structure is directly responsible for the significant improvements in LHE demonstrated by **SM315**. The dye loading on the TiO_2 films was obtained by desorbing the dyes, and the amount of dyes loaded was estimated to be 8.35×10^{-7} mol cm^{-2} for the case of the **SM315** dye. Assuming a uniform coverage on the titania without any aggregates, the **SM315** dye occupies a surface area of ~1.98 nm^2 on the TiO_2.

The steady-state fluorescence spectra for **SM371** and **SM315** are provided in the Supplementary Information (Supplementary Fig. 6). **SM371** exhibited an emission spectrum that mirrored the absorption spectrum, but that of **SM315** was broad and featureless, indicating that an enhanced ICT character of the excited state could be achieved by using the strongly electron-deficient BTD unit, thereby increasing the acceptor property of the dye[44]. Calculation of the Stokes shift for the two dyes revealed that **SM315** (1,309 cm^{-1}) experienced a greater shift than **SM371** (643 cm^{-1}). The acquisition of time-resolved luminescence in THF solution and on TiO_2 substrates provided insight into the electron injection dynamics of the two dyes (Supplementary Fig. 7). The fluorescence lifetime in solution (1.2 ns) and on TiO_2 substrates (63 and 60 ps for **SM371** and **SM315**, respectively) was identical for both dyes. This is indicative of the injection efficiency (η_{inj}) for both dyes approaching unity, as a result of efficient photoinduced electron injection from the dye into the mesoporous anode.

Electrochemical characterization. The electrochemical characterization of **SM371** and **SM315** was performed in DMF. The oxidation potential of the dyes is critical for the functioning of the DSC, as it determines the optimal cobalt redox couple to be utilized within the cell. The first oxidation potentials of **SM371** and **SM315** were both quasi-reversible, with values of +0.88 V and +0.89 V (versus NHE), respectively. The computed vertical ionization energies (of the ground-state geometry) in DMF are nearly identical for both dyes (4.86 eV and 4.85 eV for **SM371** and **SM315**, respectively), consistent with the trend observed in oxidation potential and the observation that the HOMO of **SM315** is not strongly affected by the BTD moiety.

The reduction potentials of **SM371** and **SM315** were –1.21 V and –0.99 V (versus NHE), respectively. The similarity of E_{ox} for the two dyes demonstrated a considerable advantage of the BTD-functionalized anchor, as it does not noticeably impact the oxidation potential of the dye. The BTD-functionalized anchor exclusively influenced the optical bandgap and absorption features of **SM315** (*vide supra*), allowing us to engineer the absorption features and oxidation potential of the porphyrin in a separate, modular fashion. The difference in reduction potential demonstrated the ability of the BTD unit to stabilize the LUMO, consistent with the redshift observed in the absorption spectrum of **SM315**.

Further insight into the interfacial electron transfer (that is, from the photoexcited dye to the semiconducting photoanode) was performed by intensity-modulated photoinduced absorption (PIA) measurements on TiO_2 films sensitized with **SM371** and **SM315** (Supplementary Fig. 8). Measuring the change in absorbance of the sensitized films in the absence of electrolyte (that is, acetonitrile solvent) revealed a decrease in absorbance from the Q-band, with concomitant evolution of an absorbance at 800 nm, diagnostic of formation of the porphyrin cation radical for both dyes[28]. Interestingly, the amount of dye cation radicals generated by **SM315** in the absence of the electrolyte appears to be less than for **SM371**, indicating that the injected electrons recombine with the photo-oxidized sensitizer faster for **SM315** than for **SM371**. This back reaction is facilitated by the presence of the strongly electron-deficient BTD moiety in **SM315** and is consistent with previous reports where the undesirable electron-recapture event could be partially ameliorated through the introduction of a phenyl spacer between the BTD and the anchoring group[45]. In the presence of the cobalt electrolyte, absorbance features pertaining to the porphyrin cation radical disappear entirely, indicating efficient regeneration of the porphyrins by the Co(II) species of the redox couple[6].

Photovoltaic performance. Dyes **SM371** and **SM315** were utilized in DSCs using thin (7 μm) mesoporous TiO_2 films to enable compatibility with the $[Co(bpy)_3]^{2+/3+}$ redox couple, essential in obtaining DSCs exhibiting a high V_{OC}. Figure 4 shows the *J–V* curve for the two devices measured under AM 1.5G illumination (1,000 W m^{-2} at 298 K) (data summarized in Table 2). DSCs fabricated using **SM371** gave a high V_{OC} (0.96 mV) and J_{SC} (15.9 mA cm^{-2}), achieving an overall PCE of 12.0%, a slight improvement compared to the porphyrin sensitizer YD2-o-C8, which has a similar structure[6]. Despite exhibiting a slightly lower V_{OC} of 0.91 V, the best cell made with **SM315** attained a higher J_{SC} (18.1 mA cm^{-2}) and an overall PCE of 13.0%, outperforming **SM371** as a result of the improvement in visible and near-infrared light harvesting. A histogram of 50 different devices made with SM315 dye is shown in Supplementary Fig. 10. A higher average PCE was obtained at 64% sun intensity (13.25%) than at full sun

Table 2 | Summary of photovoltaic performance data for SM371 and SM315 under AM 1.5G illumination (1,000 W m^{-2}).

Dye	V_{OC} (V)	J_{SC} (mA cm^{-2})	FF	PCE (%)
SM371	0.96	15.9	0.79	12.0
SM315	0.91	18.1	0.78	13.0

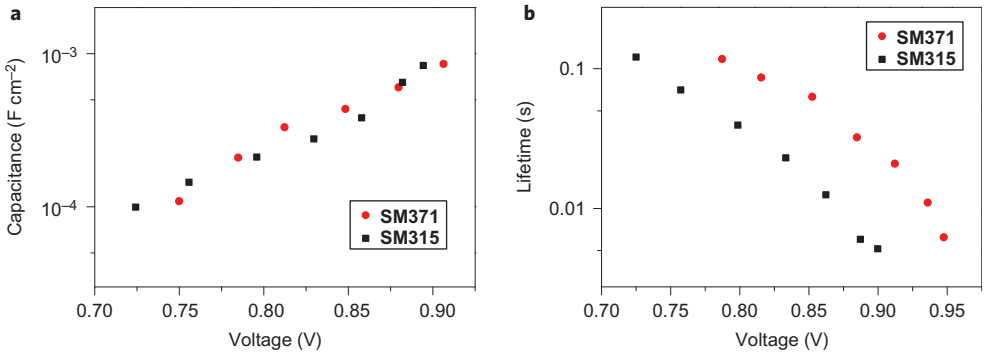

Figure 5 | Transient photocurrent and photovoltage measurements carried out on devices made with SM315 and SM371. a, Chemical capacitance and **b**, electron lifetime as a function of V_{OC} obtained through transient photocurrent and photovoltage measurements.

intensity (12.75%). The lower average at full sun intensity is mainly due to mass transport limitations of the cobalt redox mediator.

SM371 possessed a near identical photocurrent action spectrum (Fig. 4b) to that of dyes with comparable donor and acceptor substitution (that is, YD2-o-C8), with maximum incident monochromatic photon-to-electric current conversion efficiency (IPCE) values of 80% obtained at 480, 590 and 640 nm. SM315 demonstrated impressively high IPCE values across the whole visible wavelength range, maintaining a value of 80% from 450 nm to 750 nm, with the DSC harvesting light up to 800 nm, demonstrating the utility of the BTD-functionalized anchor for improvements in visible and infrared light-harvesting properties. The overlap integral of the photocurrent action spectrum with the standard AM 1.5G solar emission spectrum agrees within 2% with the measured photocurrent, demonstrating that any spectral mismatch between the simulated and true AM 1.5G sunlight is negligibly small.

Transient photovoltage and photocurrent measurements were used to investigate the origin of reduced V_{OC} for DSCs sensitized with SM315. A reduction in V_{OC} can originate from either (1) downward shift of the conduction band or (2) the enhanced recombination of injected charges in the TiO_2 film with the dye or electrolyte[6,46–48]. A downward shift of the TiO_2 conduction band (that is, displacement of the trap-state distribution function to lower energy) would cause the density of occupied states (DOS) to be higher for SM315 than for SM371[6,46–48]. Measurement of the chemical capacitance (C_μ, Fig. 5a) as a function of V_{OC} allows insight into the DOS in devices made with either dye, as C_μ and DOS are directly proportional to each other. At a given V_{OC}, C_μ is nearly identical for both dyes, ruling out a downward shift of the conduction band shift as the origin of the decreased V_{OC} in SM315-sensitized DSCs.

Measurement of the electron lifetimes as a function of V_{OC} (Fig. 5b) afforded insight into the electron recombination occurring at the TiO_2–electrolyte interface. At a given V_{OC}, the electron lifetime in cells sensitized with SM371 was two to six times longer than for SM315-sensitized DSCs. Evidence from previous work clearly demonstrates that the direct connection of the BTD group to the anchoring group accelerated conduction-band electron recapture by the sensitizer and the utilization of a phenyl spacer retards the electron recapture[45]. In this work, the PIA spectrum of SM315 (Supplementary Fig. 8b) clearly demonstrated that even with a phenyl spacer in place, the electron recapture by SM315 is faster than by SM371. This indicates that the phenyl spacer does not completely attenuate the accelerating effect of the BTD moiety on charge carrier recombination (*vide supra*). The result of the accelerated electron recapture by SM315 (compared to SM371) at the TiO_2–electrolyte interface resulted in a V_{OC} decrease of 50 mV in the device. However, this loss in V_{OC} is overcompensated by a gain in J_{SC}, resulting in the superior performance of the SM371 dye.

Long-term stability measurements were carried out on three individual devices sensitized with SM315 by subjecting them to continuous light soaking at full solar light intensity for 500 h at 298 K (Supplementary Fig. 11). The cells were kept at their maximum power point during the illumination. We obtained excellent stability over this long period, showing that the SM315 is a very stable dye and not prone to degradation, even if exposed to intense sunlight for long illumination times. During the 500 h of light soaking, devices employing SM315 underwent over one million turnovers without showing any significant loss in stability. The initial drop in PCE of ~10–20% for the three devices is attributed to desorption of a small amount of sensitizer from the TiO_2 surface, decreasing the photovoltaic performance. In the future, the introduction of stronger anchoring groups into the high-performance SM315-type design should serve to minimize any dye desorption and further improve the stability of the device.

Conclusion

Judicious molecular engineering of push–pull porphyrins has allowed the realization of two high-performance sensitizers, SM371 and SM315, exhibiting unprecedented solar-to-electric PCEs under standard AM 1.5G illumination. The green dye SM371 exhibited slightly better performance (12.0%) than the previous state-of-the-art YD2-o-C8. Introduction of the BTD-functionalized acceptor into the dye structure afforded the broadly absorbing sensitizer SM315. The enhanced visible and long wavelength absorbance properties of SM315 were rationalized by LR-TDDFT analysis. The dramatically improved absorption properties of SM315 resulted in a near-quantitative LHE across the visible spectrum and up to 800 nm, leading to greater photocurrents in the DSC device compared to SM371. Fabrication of DSCs utilizing the $[Co(bpy)_3]^{2+/3+}$ redox couple and SM315 demonstrated panchromatic light harvesting without the use of co-sensitization, leading to a record 13% PCE at full sun illumination.

Methods

Details of the synthesis and characterization of the dyes, computational investigations, DSC fabrication and photovoltaic characterization (*J–V*, IPCE, PIA, transient photovoltage/photocurrent decay, stability measurements) are described in the Supplementary Information.

Received 22 September 2013; accepted 20 December 2013; published online 2 February 2014

References

1. O'Regan, B. & Grätzel, M. A low cost, high-efficiency solar cell based on dye-sensitized colloidal TiO_2 films. *Nature* **353,** 737–740 (1991).
2. Grätzel, M. Conversion of sunlight to electric power by nanocrystalline dye-sensitized solar cells. *J. Photochem. Photobiol. A* **164,** 3–14 (2004).

3. Shah, A., Torres, P., Tscharner, R., Wyrsch, N. & Keppner, H. Photovoltaic technology: the case for thin-film solar cells. *Science* **285,** 692–698 (1999).
4. Grätzel, M. Dye-sensitized solar cells. *J. Photochem. Photobiol. C* **4,** 145–153 (2003).
5. Komiya, R. *et al.* in *Technical Digest, 21st International Photovoltaic Science and Engineering Conference* 2 C-5O-08 (2011).
6. Yella, A. *et al.* Porphyrin-sensitized solar cells with cobalt (II/III)–based redox electrolyte exceed 12 percent efficiency. *Science* **334,** 629–634 (2011).
7. Feldt, S. M. *et al.* Design of organic dyes and cobalt polypyridine redox mediators for high-efficiency dye-sensitized solar cells. *J. Am. Chem. Soc.* **132,** 16714–16724 (2010).
8. Yum, J. H. *et al.* A cobalt complex redox shuttle for dye-sensitized solar cells with high open-circuit potentials. *Nature Commun.* **3,** 631 (2012).
9. Tsao, H. N. *et al.* Cyclopentadithiophene bridged donor–acceptor dyes achieve high power conversion efficiencies in dye-sensitized solar cells based on the tris-cobalt bipyridine redox couple. *ChemSusChem* **4,** 591–594 (2011).
10. Hardin, B. E., Snaith, H. J. & McGehee, M. D. The renaissance of dye-sensitized solar cells. *Nature Photon.* **6,** 162–169 (2012).
11. Ogura, R. Y. *et al.* High-performance dye-sensitized solar cell with a multiple dye system. *Appl. Phys. Lett.* **94,** 073308 (2009).
12. Wu, H. P. *et al.* Molecular engineering of cocktail co-sensitization for efficient panchromatic porphyrin-sensitized solar cells. *Energy Environ. Sci.* **5,** 9843–9848 (2012).
13. Hardin, B. E. *et al.* Increased light harvesting in dye-sensitized solar cells with energy relay dyes. *Nature Photon.* **3,** 406–411 (2009).
14. Kuang, D. *et al.* Co-sensitization of organic dyes for efficient ionic liquid electrolyte-based dye-sensitized solar cells. *Langmuir* **23,** 10906–10909 (2007).
15. Yum, J. H., Baranoff, E., Wenger, S., Nazeeruddin, M. K. & Grätzel, M. Panchromatic engineering for dye-sensitized solar cells. *Energy Environ. Sci.* **4,** 842–857 (2011).
16. Jeong, N. C. *et al.* Effective panchromatic sensitization of electrochemical solar cells: strategy and organizational rules for spatial separation of complementary light harvesters on high-area photoelectrodes. *J. Am. Chem. Soc.* **134,** 19820–19827 (2012).
17. Shrestha, M. *et al.* Dual functionality of BODIPY chromophore in porphyrin-sensitized nanocrystalline solar cells. *J. Phys. Chem. C* **116,** 10451–10460 (2012).
18. Nattestad, A. *et al.* Highly efficient photocathodes for dye-sensitized tandem solar cells. *Nature Mater.* **9,** 31–35 (2010).
19. Yamaguchi, T., Uchida, Y., Agatsuma, S. & Arakawa, H. Series-connected tandem dye-sensitized solar cell for improving efficiency to more than 10%. *Sol. Energy Mater. Sol. Cells* **93,** 733–736 (2009).
20. Murayama, M. & Mori, T. Dye-sensitized solar cell using novel tandem cell structure. *J. Phys. D* **40,** 1664–1668 (2007).
21. Kubo, W., Sakamoto, S., Kitamura, T., Wada, Y. & Yanagida, S. Dye-sensitized solar cells: improvement of spectral response by tandem structure. *J. Photochem. Photobiol. A* **164,** 33–39 (2004).
22. Ito, S. *et al.* Fabrication of thin film dye sensitized solar cells with solar to electric power conversion efficiency over 10%. *Thin Solid Films* **516,** 4613–4619 (2008).
23. Imahori, H., Umeyama, T. & Ito, S. Large π-aromatic molecules as potential sensitizers for highly efficient dye-sensitized solar cells. *Acc. Chem. Res.* **42,** 1809–1818 (2009).
24. Bessho, T., Zakeeruddin, S. M, Yeh, C. Y., Diau, E. W. G. & Grätzel, M. Donor–acceptor-substituted porphyrins. *Angew. Chem. Int. Ed.* **49,** 6646–6649 (2010).
25. Chang, Y. C. *et al.* A strategy to design highly efficient porphyrin sensitizers for dye-sensitized solar cells. *Chem. Commun.* **47,** 8910–8912 (2011).
26. Hsieh, C. P. *et al.* Synthesis and characterization of porphyrin sensitizers with various electron-donating substituents for highly efficient dye-sensitized solar cells. *J. Mater. Chem.* **20,** 1127–1134 (2010).
27. Wu, S. L. *et al.* Design and characterization of porphyrin sensitizers with a push–pull framework for highly efficient dye-sensitized solar cells. *Energy Environ. Sci.* **3,** 949–955 (2010).
28. Lee, C. W. *et al.* Novel zinc porphyrin sensitizers for dye-sensitized solar cells: synthesis and spectral, electrochemical, and photovoltaic properties. *Chem. Eur. J.* **15,** 1403–1412 (2009).
29. Wang, C. L. *et al.* Enveloping porphyrins for efficient dye-sensitized solar cells. *Energy Environ. Sci.* **5,** 6933–6940 (2012).
30. Mathew, S. *et al.* Optical, electrochemical, and photovoltaic effects of an electron-withdrawing tetrafluorophenylene bridge in a push–pull porphyrin sensitizer used for dye-sensitized solar cells. *J. Phys. Chem. C* **115,** 14415–14424 (2011).
31. Zhou, W. *et al.* Porphyrins modified with a low-band-gap chromophore for dye-sensitized solar cells. *Org. Electron.* **13,** 560–569 (2012).
32. Susumu, K., Duncan, T. V. & Therien, M. J. Potentiometric, electronic structural, and ground- and excited-state optical properties of conjugated bis[(porphinato)zinc(II)] compounds featuring proquinoidal spacer units. *J. Am. Chem. Soc.* **127,** 5186–5195 (2005).
33. Song, H. J., Kim, D. H., Lee, T. H. & Moon, D. K. Emission color tuning of copolymers containing polyfluorene, benzothiadiazole, porphyrin derivatives. *Eur. Polym. J.* **48,** 1485–1494 (2012).
34. Lash, T. D., Chandrasekar, P., Osuma, A. T., Chaney, S. T. & Spence, J. D. Porphyrins with exocyclic rings. 13. synthesis and spectroscopic characterization of highly modified porphyrin chromophores with fused acenaphthylene and benzothiadiazole rings. *J. Org. Chem.* **63,** 8455–8469 (1998).
35. Huang, Y., Li, L., Peng, X., Peng, J. & Cao, Y. Solution processed small molecule bulk heterojunction organic photovoltaics based on a conjugated donor–acceptor porphyrin. *J. Mater. Chem.* **22,** 21841–21844 (2012).
36. Gao, P. *et al.* Facile synthesis of bulky BPTPA donor group suitable for cobalt electrolyte based dye sensitized solar cells. *J. Mater. Chem. A* **1,** 5535–5544 (2013).
37. Kasha, M., Rawls, H. R. & El-Bayoumi, M. A. The exciton model in molecular spectroscopy. *Pure Appl. Chem.* **11,** 371–392 (1965).
38. Gouterman, M. Study of the effects of substitution on the absorption spectra of porphin. *J. Chem. Phys.* **30,** 1139–1161 (1959).
39. Gouterman, M. Spectra of porphyrins. *J. Mol. Spectrosc.* **6,** 138–163 (1961).
40. Zhao, Y. & Truhlar, D. G. The M06 suite of density functionals for main group thermochemistry, thermochemical kinetics, noncovalent interactions, excited states, and transition elements: two new functionals and systematic testing of four M06-class functionals and 12 other functionals. *Theor. Chem. Acc.* **120,** 215–241 (2008).
41. Duffy, N. W., Dobson, K. D., Gordon, K. C., Robinson, B. H. & McQuillan, A. J. *In situ* infrared spectroscopic analysis of the adsorption of ruthenium (II) bipyridyl dicarboxylic acid photosensitisers to TiO_2 in aqueous solutions. *Chem. Phys. Lett.* **266,** 451–455 (1997).
42. Jones, F., Farrow, J. B. & van Bronswijk, W. An infrared study of a polyacrylate flocculant adsorbed on hematite. *Langmuir* **14,** 6512–6517 (1998).
43. Kira, A. *et al.* Effects of π-elongation and the fused position of quinoxaline-fused porphyrins as sensitizers in dye-sensitized solar cells on optical, electrochemical and photovoltaic properties *J. Phys. Chem. C* **114,** 11293–11304 (2010).
44. Longhi, E. *et al.* Metal-free benzodithiophene-containing organic dyes for dye-sensitized solar cells. *Eur. J. Org. Chem.* **2013,** 84–94 (2013).
45. Haid, S. *et al.* Significant improvement of dye-sensitized solar cell performance by small structural modification in π-conjugated donor–acceptor dyes. *Adv. Funct. Mater.* **22,** 1291–1302 (2012).
46. Barnes, P. R. F. *et al.* Interpretation of optoelectronic transient and charge extraction measurements in dye-sensitized solar cells. *Adv. Mater.* **25,** 1881–1922 (2013).
47. O'Regan, B. C. & Lenzmann, F. Charge transport and recombination in a nanoscale interpenetrating network of *n*-type semiconductors: transient photocurrent and photovoltage studies of TiO_2/dye/CuSCN photovoltaic cells. *J. Phys. Chem. B* **108,** 4342–4350 (2004).
48. O'Regan, B. C. *et al.* Measuring charge transport from transient photovoltage rise times: a new tool to investigate electron transport in nanoparticle films. *J. Phys. Chem. B* **110,** 17155–17160 (2006).

Acknowledgements

The research leading to these results received funding from Solvay Fluor GmbH, the European Union Seventh Framework Programme (FP7/2007–2013) under grant agreement 'ENERGY-261920, ESCORT' and SSSTC (Sino-Swiss Science and Technology Cooperation), and the European Community's Seventh Framework Programme (FP7/2007–2013) under grant agreement no. 246124 of the SANS project. M.G. thanks the European Research Council (ERC) for supporting part of this work under the advanced research grant (no. 247404) MESOLIGHT. A.Y. acknowledges the Balzan Foundation for support as part of the Balzan prize awarded to M.G. in 2009. M.K.N. acknowledges the World Class University programme, Photovoltaic Materials, Department of Material Chemistry, Korea University, Chungnam, 339-700, Korea, funded by the Ministry of Education, Science and Technology through the National Research Foundation of Korea (no. R31-2008-000-10035-0).

Author contributions

A.Y. and S.M. proposed the research. S.M. synthesized and characterized the dyes with assistance from P.G. A.Y. fabricated and optimized the DSCs and conducted all the photovoltaic characterization. Electrochemical characterization was performed by P.G. R.H.B performed photo-physical characterization and assisted in interpreting the results with assistance from A.Y. and M.G. R.H.B designed the instruments and contributed to interpreting the results. B.F.E.C. and N.A.A. performed the computational characterization, with I.T. and U.R. contributing to the analysis and interpretation of the results. M.K.N. is responsible for overseeing the sensitizer project. M.G. directed the scientific research for this work and assumed all correspondence with the editor and reviewers. S.M. and M.G. prepared the manuscript, with invaluable contributions from A.Y., R.H.B., M.K.N., B.F.E.C., N.A.A., I.T. and U.R.

Additional information

Supplementary information and chemical information are available in the online version of the paper. Reprints and permissions information is available online at www.nature.com/reprints. Correspondence and requests for materials should be addressed to M.G.

Competing financial interests

The authors declare no competing financial interests.